Fundamental understanding of NBTI degradation mechanism in IGZO channel devices

Ying Zhao*[1], Pietro Rinaudo*[1], Adrian Chasin, Brecht Truijen, Ben Kaczer, Nouredine Rassoul, Harold Dekkers, Attilio Belmonte, Ingrid De Wolf[1], Gouri Kar and Jacopo Franco
imec, Leuven, Belgium, email: ying.zhao@imec.be, [1] also at KU Leuven, Belgium, *equal contributions

***Abstract*— Negative bias temperature instability (NBTI) of IGZO thin film transistors (TFTs) with different channel thicknesses(t_{IGZO}) and gate lengths is studied. Four main NBTI characteristics are observed: (1) the threshold voltage shift appears to be almost independent of the gate stress voltage (above a given stress voltage determined by the t_{IGZO}), and shows (2) a large activation energy (i.e., a strong temperature dependence) and (3) a steep time kinetics (i.e., a large power-law time exponent), while (4) the NBTI relaxation rate is reduced for increasing temperatures below 200°C. By combining TCAD simulations with experimental data modelling, these peculiar features can be explained by an oxide-field-driven hydrogen release from the gate-dielectric, inducing additional IGZO donor doping and a subsequent negative V_{th} shift. The latter mechanism is observed to be analogous to the negative V_{th} shift reported during PBTI stress at elevated temperature in IGZO devices [1].**

***Index Terms*—IGZO, NBTI, negative shift, oxide-field-driven hydrogen release.**

I. Introduction

IGZO (Indium Gallium Zinc Oxide) TFTs are considered potential key components in advancing next-gen semiconductor evolution, as they offer distinct advantages such as BEOL compatibility, good uniformity for channel deposition, low leakage current and low cost. In particular, they are promising for DRAM applications and for monolithic 3D integration [2-5]. Accompanying the rapid development of IGZO devices is the growing concern regarding their reliability [1, 6-9]. Unlike Si devices, a negative V_{th} shift during P(positive)BTI stress has been identified as the process limiting the device's lifetime at high temperatures [1]. Until now, fundamental and systematic study about NBTI degradation of IGZO is still lacking. Previous studies on negative bias stress and negative bias illumination stress in IGZO transistors ascribed degradation to IGZO film itself, hole trapping from valence band [10], impact of sub-gap states like peroxides [11] or ionized oxygen vacancies [12], without considering the role of gate-dielectric.

In this work, the NBTI of IGZO devices is thoroughly characterized and investigated. We measure NBTI at different temperatures (T) in back-gated (BG) IGZO devices with various channel thicknesses. TCAD simulations are performed to get insights on the device electrostatics at the stress conditions used in the experiments. Relaxation dynamics are modelled giving additional understanding on the degradation mechanism.

II. Experiments and Results

A. Device fabrication and Measurement method

BG IGZO TFTs used in this research are fabricated on a 300mm wafer platform. Silicon(p++) is used for backside gate electrode, upon which a 10 nm Al_2O_3 dielectric layer is deposited via Atomic Layer Deposition (ALD) at 300°C. Three different IGZO channel thicknesses (t_{IGZO}=5nm, 10nm, 20nm) are deposited by a Physical Vapor Deposition (PVD) process. Next, the encapsulation layer (SiO_2), and S/D contacts (TiN/W) are formed subsequently. Finally, the devices are annealed at 350°C under O_2 environment for one hour. Devices with two gate lengths of 10µm and 200nm (W_G=10µm) are used for the NBTI study, whose structure is depicted in Fig.1(a).

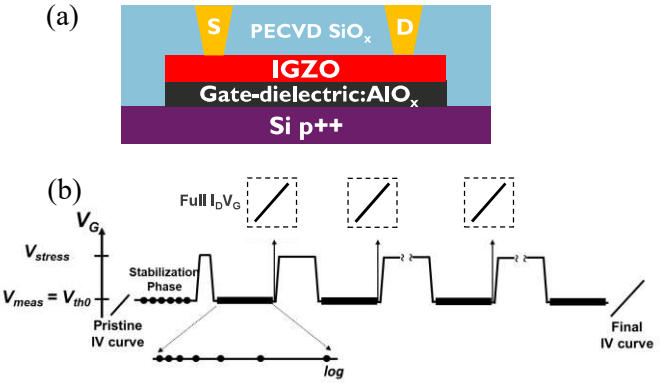

Figure1 - (a) BG IGZO TFTs' structure. (b) Schematic of the modified version of eMSM sequence. The standard eMSM is the sequence without full IV measurement after each stress/recovery cycle.

Electrical stress experiments (both for PBTI and NBTI) are carried out by the so-called extended Measure-Stress-Measure (eMSM) methodology, to record as much stress and relaxation data during one measurement as possible (further details available in [13]). We also use a modified version of the eMSM sequence [14] for NBTI study, in which a full transfer characteristic in linear (V_d=50mV) condition is measured after each stress/recovery cycle, as shown in Fig. 1(b). This method enables us to closely monitor the device's operational stability under heightened bias conditions, including extra degradation of mobility or subthreshold characteristics. All the measurements are run in a fully dark environment excluding light impact.

B. Device characteristics

Before BTI study, we first assess the time-zero device characteristics of initial V_{th} (V_{th0}), subthreshold slope (SS) and

mobility of various IGZO devices, given in Fig. 2(a)-(c) with t_{IGZO}=5nm, 10nm, 20nm. Among them V_{th} is determined at a fixed current level with I_{th}=10nA. *SS* and mobility are calculated from $SS = \frac{d \log I_D}{dV_G}$ and g_m peak where $g_m = \frac{dI_D}{dV_G}$. Notably, the devices with 20nm IGZO exhibit the most negative V_{th0} and the poorest *SS*, while 10nm-IGZO devices show superior mobility performance. Also, a temperature increase from 25°C to 125°C leads to degradation in *SS* for all devices alongside an enhancement in their mobility, typical for amorphous oxide semiconductor channels.

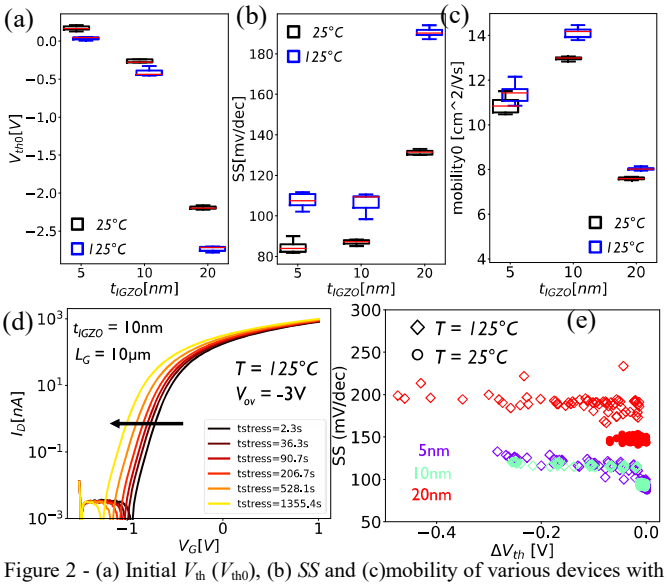

Figure 2 - (a) Initial V_{th} (V_{th0}), (b) *SS* and (c)mobility of various devices with different IGZO thicknesses used for time dependent BTI measurement under 25°C and 125°C. (d) Raw IV curves after each NBTI stress phase at V_{ov} = $V_{g\_applied}$−V_{th0}=-3V, showing only a "rigid" shift of the transfer characteristics. (e) *SS* as a function of the NBTI-induced ΔV_{th}, showing negligible changes also for large V_{th} changes.

Further analysis is conducted through transfer I-V curve measurements during BTI measurement via the modified eMSM method. Figure 2 (d) presents an example of how the I-V curve evolves with stress time on a 10nm thick IGZO channel biased at V_{ov} = -3V at 125°C. It exhibits a clear "rigid" shift towards negative voltages, without any *SS* change. Furthermore, we extract the *SS* of all devices and stress phases as a function of V_{th} shift, as shown in Fig.2(e). The lack of *SS* degradation during a large range of V_{th} degradation also confirms that NBTI induces mainly a rigid shift of the IV curve, in contrast to Si technology.

C. BTI results

The typical ΔV_{th} kinetics for both NBTI and PBTI are shown in Fig. 3 across different t_{IGZO} of IGZO. As compared with the complex, non-monotonic behavior observed in PBTI, negative stress voltages consistently induce negative V_{th} shifts, which are more pronounced in thicker IGZO films. This phenomenon and trend are evident at both 25°C [Fig.3 (a)] and at 125°C [Fig.3 (b)]. The V_{th} shifts of NBTI are at the same magnitude as PBTI under 25°C, while they show a more pronounced V_{th} shift than PBTI under 125°C. Consistently, NBTI exhibits thermal activation in Fig.4, inducing larger

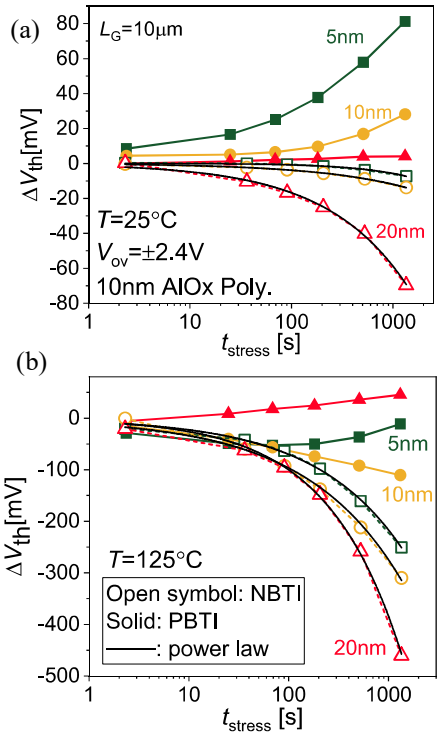

Figure 3 - ΔV_{th} as function of stress time (time kinetics) of NBTI (open symbols) and PBTI (solid) under *T*=25°C (a) and 125°C (b) both at V_{ov}=-2.4V. NBTI increases for thicker IGZO films. At 125C, NBTI is more pronounced than PBTI. All the NBTI curves can be fitted by power laws (black lines), see Eq. (1).

negative shifts as temperature increases. All the ΔV_{th} time kinetics of NBTI can be fitted by a semi-empirical model as the black lines shown in Fig.3 and Fig.4,

$$\Delta V_{th} = A \times t_{stress}^{n}, \qquad (1)$$

where n is time exponent derived from a well approximation of tail of log normal distribution of capture times, the larger n the

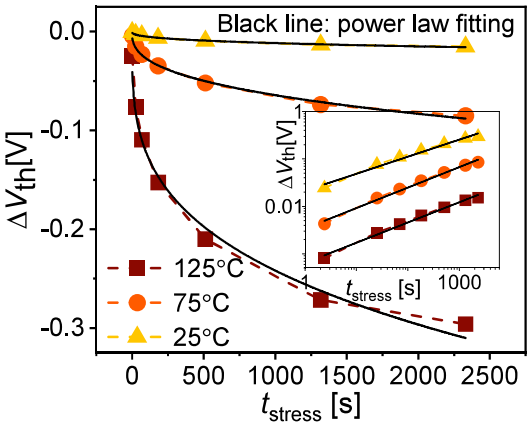

Figure 4 - The time kinetics of NBTI in a 10nm IGZO channel at different stress temperatures, with a higher temperature inducing a larger ΔV_{th}. A power law fit with a temperature-dependent pre-factor is applicable for estimating the activation energy of the process [Eq.(1)]. Inset shows the log scale of the same time kinetics of NBTI.

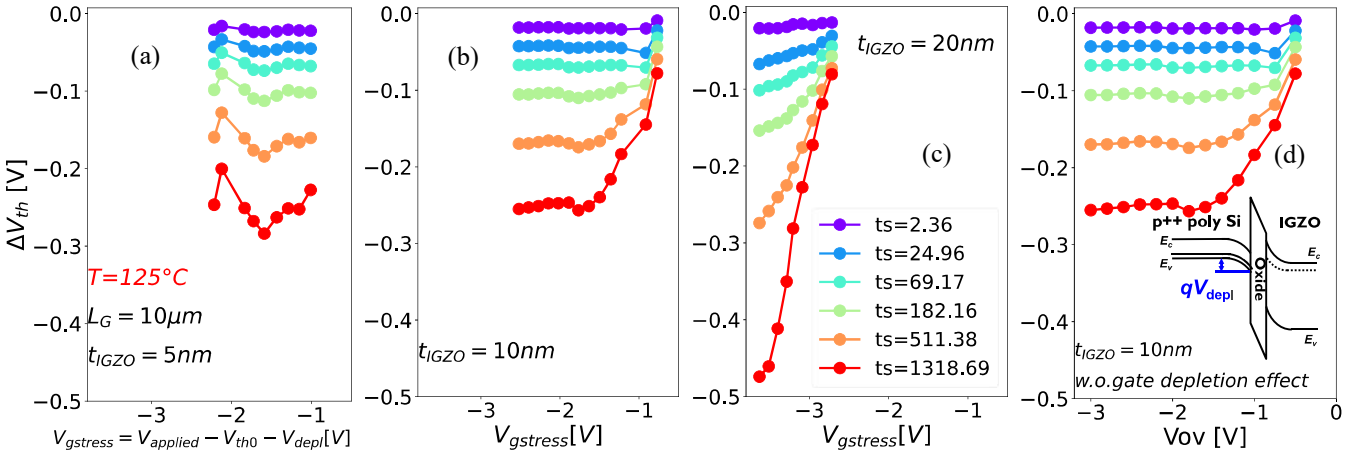

Figure 5 - Stress voltage dependence of NBTI for 5nm (a), 10nm (b) and 20nm (c) thick IGZO under T=125°C. The thicker the IGZO film is, the stronger the stress voltage dependence. V_{g_stress} used in figures are corrected by gate depletion voltage V_{depl}: $V_{g\_stress} = V_{g\_applied} - V_{th0} - V_{depl}$. (d) Stress voltage dependence of NBTI without accounting for gate depletion for 10nm IGZO as an example, $V_{ov} = V_{g\_applied} - V_{th0}$, where saturation can be still observed. Inset: band diagram depicting the gate depletion.

slower the charge trapping (capture) process. The pre-factor A in Eq.(1) denotes ΔV_{th} at t_{stress}=1s and exhibits a thermally activated behavior $A = A_0 \times \exp\left(-\frac{E_a}{k_B T}\right)$ where E_a is the activation energy. Further detailed analysis of model parameters together with possible physical mechanism behind NBTI will be discussed in subsequent part.

An unusual correlation between ΔV_{th} on V_{g_stress} is observed in Fig.5, showing a strongly dependence on the t_{IGZO}. For the thickest IGZO (20nm), a continuous ΔV_{th} increase with V_{g_stress} is observed [Fig.5(c)], whereas for a 10nm thick channel the ΔV_{th} appears to saturate above a given V_{g_stress} [Fig.5(b)]. In contrast, a negligible voltage dependence is observed for the thinnest channel (5nm), in the considered V_{g_stress} range <-1V [Fig.5(a)]. To make the dependence of stress voltage convincing, the stress voltages used in NBTI assessment are first corrected for poly-Si gate depletion effect in IGZO devices by an estimation based on the expected gate doping level (10^{19} cm^{-3}): when a negative bias is applied on Silicon(p++) gate ($V_{g\_applied}$), leading to gate depletion [inset of Fig.5(d)], part of the applied voltage (V_{depl}) drops across the gate, and it should be accounted for estimating the oxide field, $V_{g\_stress} = V_{g\_applied} - V_{th0} - V_{depl}$. From Fig.5(b) and (d), it is clear to see that the saturation of V_{g_stress} dependence remains irrespective of the gate depletion consideration.

III. TCAD SIMULATIONS

TCAD simulations are performed to elucidate the peculiar V_{g_stress} dependence shown in Fig.5. Figure 6 shows the simulated gate-dielectric electric field (E_{ox}) with varying V_{g_stress} at two representative locations: the center of the channel [Fig.6(a)] and the region under S/D[Fig.6(b)]. For the PBTI case, i.e., V_{g_stress}>0, E_{ox} has the same voltage dependence at any location. In contrast for V_{g_stress}<0 (NBTI regime) E_{ox} shows a voltage dependence only in the regions under S/D, while a clear saturation of E_{ox} is observed in the center of the channel above a given V_{g_stress}. Additionally, it is revealed that thicker IGZO films correspond to larger E_{ox} and larger saturating V_{g_stress} in Fig.6 (a) (and thus ΔV_{th} under NBTI stress [Fig.3 and Fig.5]). The E_{ox} saturation elucidated by TCAD simulations aligns very well with the experimental findings of ΔV_{th} Fig.5.

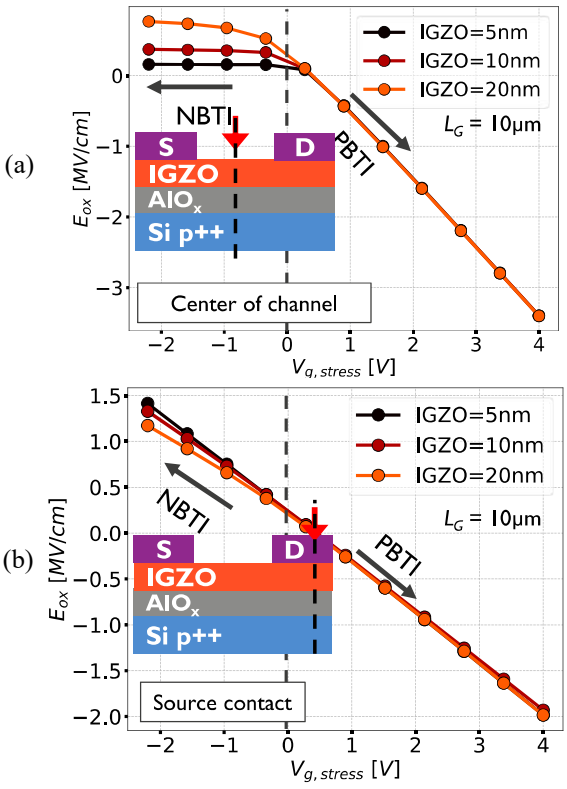

Figure 6 - TCAD simulation results of gate-dielectric field E_{ox} as a function of stress voltage V_{g_stress}: (a) E_{ox} cut at center of channel region; (b) E_{ox} cut at region under S/D. V_{g_stress} dependence of E_{ox} gets weaker for thinner IGZO in the center of the channel, as the thinner channel reaches full depletion at lower voltage (E_{ox} plateau). Notice the plateau at a larger E_{ox} for the thicker IGZO films, due to the larger depletion charge at full depletion.

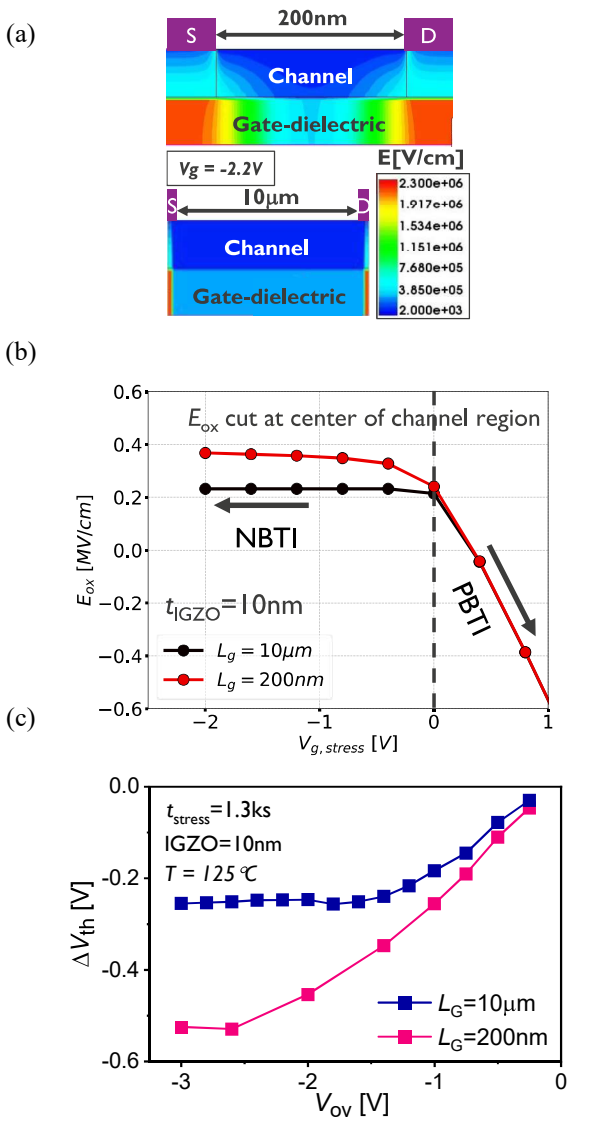

Figure 7 - (a) 2D distribution of electric field in short(upper) and long(lower) devices simulated by TCAD, showing higher E_{ox} in the regions under S/D. The shorter device experiences increased E_{ox} in the center of the channel due to larger impact from the regions under S/D. (b) TCAD simulation results of E_{ox} as a function of V_{g_stress} for different gate length (L_g=10μm and L_g=20nm). Shorter device has larger E_{ox} and stronger voltage dependence. (c) Voltage dependence of ΔV_{th} at t_{stress}=1.3ks for short and long devices from experiments. The shorter device shows larger degradation and stronger voltage dependence, in agreement with the simulated voltage dependence of E_{ox} in (b).

This finding is further supported by comparing E_{ox} and ΔV_{th} in different gate length devices. The 2D distribution of electric field in short and long devices is depicted in Fig.7(a), highlighting that the regions under S/D have larger electric field than center of channel and the shorter device is overall more impacted by the S/D regions. This leads to larger E_{ox} and more negative voltage of V_{g_stress} at which degradation saturated for shorter devices as compared to the longer device [Fig.7(b)]. This predicted simulation results also verified experimentally in Fig.7(c), the shorter device has an increased degradation and enhanced V_{g_stress} sensitivity (postponed E_{ox} saturation). The consistent correlation between E_{ox} and ΔV_{th}

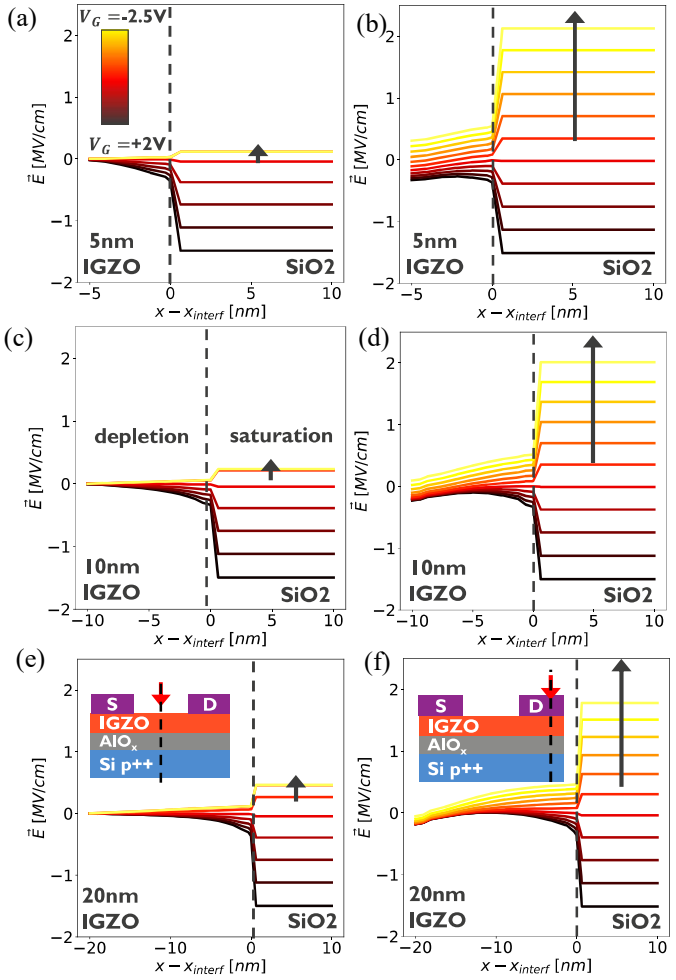

Figure 8 – TCAD simulation results of electric field changing with the distance x vertical to the interface: (a), (c) and (e) are cut at center of channel region where a clear saturation showing for both electric field of IGZO film and gate dielectric when IGZO film full depleted; (b), (d) and (f) are cut at region under S/D, where the electric field drops normally.

confirms NBTI of IGZO is governed by E_{ox}. The apparent saturation of the NBTI voltage dependence is solely related to the lack of inversion of the IGZO semiconductor [15]: once the channel is fully depleted, any further increase in gate voltage cannot result in a corresponding increase of the channel potential, and thus the E_{ox} does not increase any further in the channel region, away from the grounded S/D contacts, as shown in Fig. 8 that depicts the evolution of electric field along channel. The degree of depletion is governed by the IGZO thickness, which, in turn determines the intensity of saturation of E_{ox} and ΔV_{th}.

IV. Relaxation Kinetics and Analysis

The ΔV_{th} recovery as a function of the so-called universal relaxation time t_{relax}/t_{stress} [13] is shown in Fig. 9. Long (up to 10ks) and short recovery processes after varying stress times are monitored under different temperatures. Degradations continue to recover post-stress voltage removal and show a retarded recovery onset at higher temperatures. The recovery traces are fitted by the universal relaxation function (URF) [16]

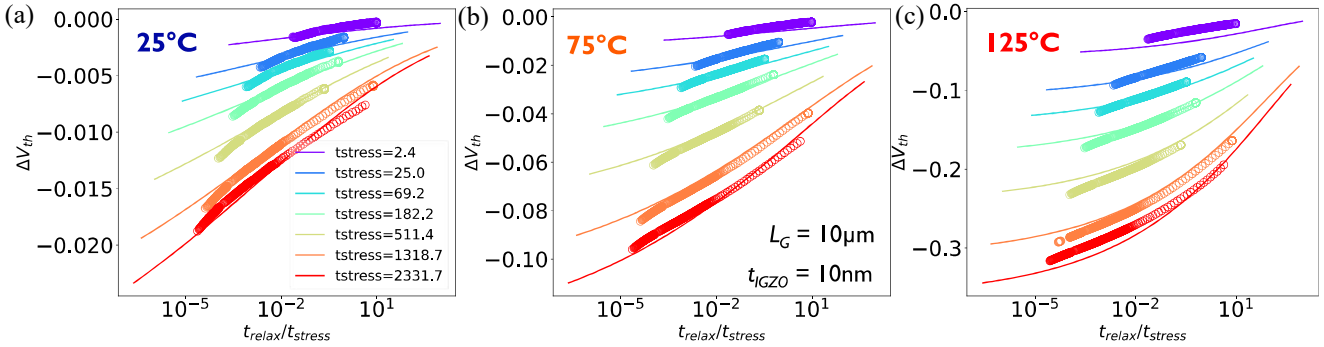

Figure 9 - (a) Experimental recovery traces fitted with the URF model [Eq. (2)] describing ΔV_{th} as a function of t_{relax}/t_{stress} at T = 25°C (a), 75°C (b) and 125°C (c), V_{ov} = -2.4V. The degradation shows recovery after stress at all temperatures; notice the retarded recovery onset at higher temperatures.

$$\Delta V_{th} = A_{0\_URF} \times \exp\left(-\frac{E_a}{k_B T}\right) \times t_{stress}^{n_{URF}} \times \frac{1}{1+B\left(\frac{t_{relax}}{t_{stress}}\right)^{\beta}}, \quad (2)$$

where β represents the spread of emission times and parameter B represents the inverse of the average emission time constant. The larger the B is, the lower the emission time and the faster the emission process. B also exhibits a thermally activated behavior $B = B_0 \times \exp\left(-\frac{E_{a\_B}}{k_B T}\right)$ where E_{a_B} is the activation energy of B.

Parameter extraction from stress kinetics [Eq.(1)] and URF fitting deepens our understanding of the NBTI process. In Fig. 10 (a) and (b), time exponents n derived from Eq.(1) for various IGZO thicknesses and temperatures, fall between 0.3 to 0.6, without obvious thickness and temperature dependence. The values of n of IGZO NBTI significantly exceed the n values commonly observed for typical range of e-/h+ trapping in gate dielectrics [1], indicating a retarded degradation process, with less distributed characteristic times.

The temperature-dependent pre-factor A (ΔV_{th} at t_{stress}=1s) in Eq.(1) [Fig.10(c)] reveals an apparent Arrhenius activation energy E_a ≥370meV, far exceeding the 30-100meV range of typical gate oxide charge trapping. Considering the larger n, the degradation of IGZO NBTI may not be attributed to normal e-/h+ capturing. Notice that the actual activation energy of the underlying process is best estimated from the ΔV_{th} parameters as $E_{a\_rele}=E_a/n$ >1.2eV.

From temperature dependence of B [Fig.10 (d)], an unusual negative activation energy of B, E_{a_B}, is extracted, implying a larger emission time and consequently, a slower emission process at higher temperatures. This contrasts with the positive E_{a_B} in typical charge trapping but mirrors the negative E_{a_B} associated with hydrogen (H) release process after incorporation in IGZO observed for PBTI's negative shift [1].

Furthermore, according to the gate-side H release model previously developed for the permanent component of NBTI in Si devices [17], the value of E_{a_rele} (>1.2eV) in our case roughly matches the energy barrier needed for H release from the gate dielectric following electron injection from the gate (1.2~1.5eV) [17]. Thus the evidence above about larger n than charge trapping, negative E_{a_B} and matched value of E_{a_rele} points to the physical mechanism behind NBTI's negative shift of IGZO. H, stored in the gate dielectric as protons [Fig.11(a)], can be effectively neutralized through an oxide-field-driven trapping process. In NBTI, the oxide field generated by applied negative bias lowers the energy barrier for trapping of gate electrons at the H storage sites [Fig.11(b)], while for PBTI it lowers the energy barrier for trapping channel electrons at the H storage sites. The neutralized H_0 is then released over a

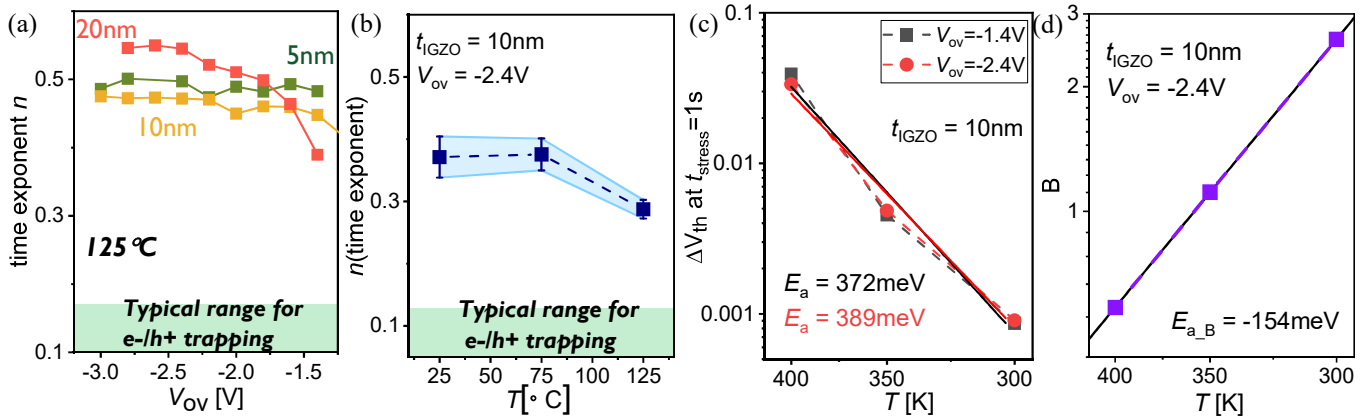

Figure 10 - The relationship between degradation kinetics (time exponent n) and overdrive voltage (V_{ov}=$V_{g\_applied}$-V_{th0}) for 5nm, 10nm and 20nm IGZO films. (b)Temperature dependence of time exponent n. (c) Apparent Arrhenius activation of ΔV_{th} at t_{stress}=1s (pre-factor A in Eq. (1)) under different stress V_{ov}. (d) Temperature dependence of B (Eq. (2)) from which a negative E_{a_B} can be extracted (i.e., retarded recovery at higher temperature).

thermal barrier, whose energy range is approximately 1.2 to 1.5 eV [Fig.11 (c)]. Following this release, the hydrogen diffuses rapidly (i.e., not a rate limiting step in thin dielectrics) towards the IGZO channel, independent of the polarity of the gate bias. Finally, the H_0 gets incorporated in IGZO as an additional donor doping, releases an electron in the film, and thus causes a negative ΔV_{th} in NBTI. Note that H can be apparently released back from the IGZO film after stress removal, inducing a recovery of the negative ΔV_{th}, consistent with the observation for the PBTI case [1]. Further investigation is necessary to shed light on the microscopic process governing the recovery; we speculate the retarded recovery at elevated temperature might be due to a more stable hydrogen bonding configuration attainable during stress at elevated temperature.

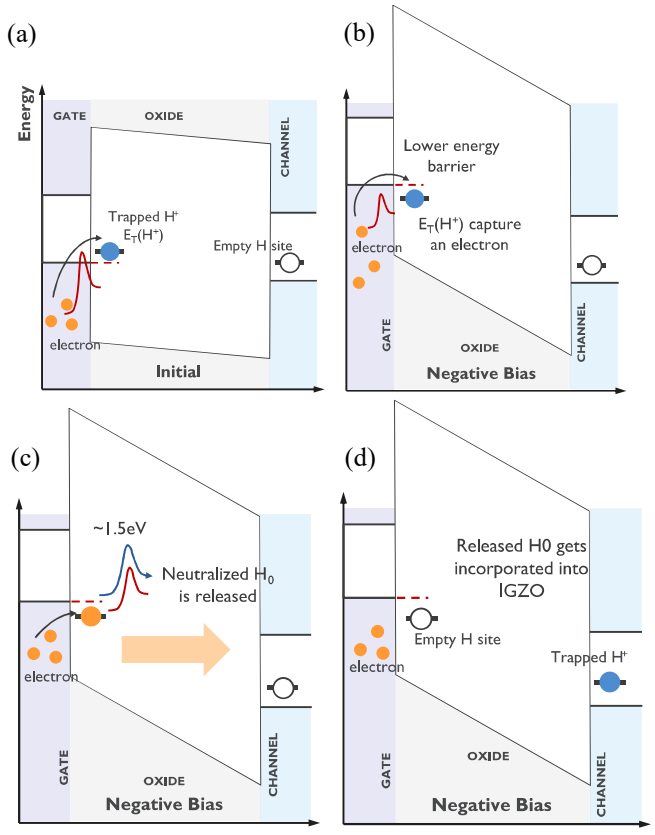

Figure 11 – Schematic of gate-side-H-release physical mechanism: A trapped H+ at the gate side (a) can be neutralized during negative stress by capturing an electron from gate(b) because of the lower energy barrier under negative bias, then released as H_0 over a barrier(~1.5eV, consistent with the experimentally extracted E_a) (c), diffusing to the channel where it gets incorporated in the IGZO film (d). Based on [17].

V. Conclusion

Comprehensive analysis of IGZO NBTI, using diverse devices and conditions, coupled with TCAD and degradation kinetic modeling, reveals a gate-dielectric field-driven behavior. The relaxation kinetics and stress voltage dependence across IGZO thicknesses and gate lengths further suggest that hydrogen released from the gate dielectric is the key agent in the doping mechanism triggering IGZO's negative Vth shift during both NBTI and PBTI stresses.

References

[1] A. Chasin, J. Franco, K. Triantopoulos, H. Dekkers, N. Rassoul, A. Belmonte, ... & G. S. Kar, "Understanding and modelling the PBTI reliability of thin-film IGZO transistors," in Proc. of the 2021 IEEE International Electron Devices Meeting (IEDM), Dec., pp. 31-1.

[2] A. Belmonte, H. Oh, N. Rassoul, G. L. Donadio, J. Mitard, H. Dekkers, ... & G. S. Kar, "Capacitor-less, long-retention (> 400s) DRAM cell paving the way towards low-power and high-density monolithic 3D DRAM," in Proc. of the 2020 IEEE International Electron Devices Meeting (IEDM), Dec., pp. 28-2.

[3] K. Huang, X. Duan, J. Feng, Y. Sun, C. Lu, C. Chen, ... & M. Liu, " Vertical Channel-All-Around (CAA) IGZO FET under 50 nm CD with High Read Current of 32.8 μA/μm (Vth+ 1 V), Well-performed Thermal Stability up to 120°C for Low Latency, High-density 2T0C 3D DRAM Application," in Proc. of the 2022 IEEE Symposium on VLSI Technology and Circuits, June, pp. 296-297.

[4] S. Subhechha, N. Rassoul, A. Belmonte, R. Delhougne, K. Banerjee, G. L. Donadio, ... & G. S. Kar, "First demonstration of sub-12 nm Lg gate last IGZO-TFTs with oxygen tunnel architecture for front gate devices" In 2021 IEEE Symposium on VLSI Technology, June, pp. 1-2

[5] W. Lu, Z. Zhu, K. Chen, M. Liu, B.M. Kang, X. Duan, ... & M. Liu, "First Demonstration of Dual-Gate IGZO 2T0C DRAM with Novel Read Operation, One Bit Line in Single Cell, ION=1500 μA/μm@ VDS=1V and Retention Time> 300s", in Proc. of the 2022 IEEE International Electron Devices Meeting (IEDM), Dec., pp. 26-4.

[6] P. Rinaudo, A. Chasin, J. Franco, Z. Wu, N. Rassoul, R. Delhougne, ... & G. S. Kar, "Degradation mapping of IGZO TFTs," in Proc. of the 2022 IEEE International Integrated Reliability Workshop (IIRW), Oct., pp. 1-5.

[7] Q. Kong, G. Liu, C. Sun, Z. Zheng, D. Zhang, J. Zhang, ... & X. Gong, "New Insights into the Impact of Hydrogen Evolution on the Reliability of IGZO FETs: Experiment and Modeling," in Proc. of the 2022 International Electron Devices Meeting (IEDM), Dec., pp. 30-2.

[8] Z. Bai, Y. Zhao, J. Wang, J., D. Liu, Y. Shan, Z. Guo, ... & L. Li, "High mobility achieved in InGaZnO TFT with vacuum-gap as insulating layer", Applied Physics Letters,121 (26), 2022.

[9] Z. Wu, A. Chasin, J. Franco, S. Subhechha, H. Dekkers, Y. V. Bhuvaneshwari, ... & G. S. Kar, "Characterizing and Modelling of the BTI Reliability in IGZO-TFT using Light-assisted IV Spectroscopy," in Proc. of the 2022 International Electron Devices Meeting (IEDM), Dec., pp. 30-1.

[10] S. Y. Lee, S. J. Kim, Y. W. Lee, W. G. Lee, K. S. Yoon, J. Y. Kwon, & M. K. Han, "The effect of the photo-induced carriers on the reliability of oxide TFTs under various intensities of light," IEEE Electron Device Letter, vol. 33, no. 2, pp. 218-220, 2012.

[11] J. Gwang Um, M. Mativenga, P. Migliorato, & J. Jang, "Increase of interface and bulk density of states in amorphous indium gallium zinc oxide thin film transistors with negative-bias-under-illumination-stress time," Applied Physics Letters, vol. 101, no. 11, 2012.

[12] A. de Jamblinne de Meux, G. Pourtois, J. Genoe, & P. Heremans, "Effects of hole self-trapping by polarons on transport and negative bias illumination stress in amorphous-IGZO," Journal of Applied Physics, vol. 123, no. 16, 2018.

[13] B. Kaczer, T. Grasser, J. Roussel, J. Martin-Martinez, R. O'Connor, B. J. O'sullivan, & G. Groeseneken, "Ubiquitous relaxation in BTI stressing—New evaluation and insights," in Proc. of the 2008 IEEE International Reliability Physics Symposium (IRPS), Apr., pp. 20-27.

[14] A. Chasin, E. Bury, B. Kaczer, J. Franco, P. Roussel, R. Ritzenthaler, ... & A. Mocuta, "Complete degradation mapping of stacked gate-all-around Si nanowire transistors considering both intrinsic and extrinsic effects", In 2017 IEEE International Electron Devices Meeting (IEDM) Dec., pp. 7-1.

[15] T. Kamiya, K. Nomura, & H. Hosono, "Electronic structure of the amorphous oxide semiconductor a-InGaZnO4–x: Tauc–Lorentz optical model and origins of subgap states," Physica Status Solidi (a), vol. 206, no. 5, pp. 860-867, 2009.

[16] T. Grasser et al., "The 'permanent' component of NBTI: Composition and annealing," in the 2011 IEEE International Reliability Physics Symposium (IRPS), Apr., pp. 6A-2.

[17] T. Grasser, M. Waltl, Y. Wimmer, W. Goes, R. Kosik, G. Rzepa, ... & B. Kaczer, "Gate-sided hydrogen release as the origin of 'permanent' NBTI degradation: From single defects to lifetimes," in Proc. of the 2015 IEEE International Electron Devices Meeting (IEDM), Dec., pp. 20-1.